Demand-side Management Based on Model Predictive Control in Distribution Network for Smoothing Distributed Photovoltaic Power Fluctuations

Jian Xu, *Senior Member*, *IEEE*, Haobo Fu, Siyang Liao, *Member*, *IEEE*, Boyu Xie, Deping Ke, Yuanzhang Sun, *Senior Member*, *IEEE*, Xiong Li, and Xiaotao Peng

***Abstract*—With the rapid increase of distributed photovoltaic (PV) power integrating into the distribution network (DN), the critical issues such as PV power curtailment and low equipment utilization rate have been caused by PV power fluctuations. DN has less controllable equipment to manage the PV power fluctuation. To smooth the power fluctuations and further improve the utilization of PV, the regulation ability from the demand-side needs to be excavated. This study presents a continuous control method of the feeder load power in a DN based on the voltage regulation to respond to the rapid fluctuation of the PV power output. PV power fluctuations will be directly reflected in the point of common coupling (PCC), and the power fluctuation rate of PCCs is an important standard of PV curtailment. Thus, a demand-side management strategy based on model predictive control (MPC) to mitigate the PCC power fluctuation is proposed. In pre-scheduling, the intraday optimization model is established to solve the reference power of PCC. In real-time control, the pre-scheduling results and MPC are used for the rolling optimization to control the feeder load demand. Finally, the data from the field measurements in Guangzhou, China are used to verify the effectiveness of the proposed strategy in smoothing fluctuations of the distributed PV power.**

***Index Terms*—Demand-side management, multi-time-scale optimization, power fluctuation smoothing, load control, model predictive control (MPC).**

I. Introduction

THE capacity of distributed photovoltaic (PV) in distribution networks (DNs) has rapidly increased in recent years [1]. Because the PV output is affected by uncertain factors such as clouds and irradiance, its power drastically fluctuates in a short time [2]. There is a lack of effective flexible regulation methods to cope with the fluctuation of the PV output in the existing DN, leading to the low utilization of equipment, voltage flickering, and curtailment of PV power [3]. Therefore, certain transmission system operators (TSOs) such as State Grid Corporation of China (SGCC), China Southern Power Grid Company Limited, and North American Electric Reliability Corporation have developed new grid codes that limit the ramp rate at the PV point of interconnection (POI) within 10% per minute [4], [5]. A DN normally covers a small area, and the external environment around each distributed PV is similar. When the irradiance abruptly changes, the fluctuation of the distributed PV power is superimposed, causing the power of the point of common coupling (PCC) in the DN to fluctuate drastically. Therefore, to reduce the impact of power fluctuations, it is necessary to use efficient and rapid power control methods to smooth PCC power fluctuations.

It is a traditional control method to use the rapid regulation ability of energy storage systems (EESs) and distributed generators (DGs) such as microturbines and diesel engines to smooth PV power fluctuations [6], [7]. However, owing to the high cost of DGs and ESSs, the operating costs in the DN increase as the distributed PV penetration increases. The static load model is commonly used in power systems to describe loads and reveal the coupling relationship between the load power and voltage [8], [9]. Certain TSOs currently control the active power by reducing the voltage to reduce the energy consumption [10]-[12]. Using the coupling characteristics between the voltage and power, the active power regulation can be rapid and continuous by regulating the voltage, so as to save the cost of deploying EESs. The topology of the DN presents the radiation shape in units of feeders; therefore, this study uses the characteristics between the load and voltage to achieve feeder-level load control by regulating the feeder voltage.

The continuous regulation performance of the voltage-regulating equipment is the premise of feeder-level load control.

Manuscript received: September 18, 2021; revised: January 27, 2022; accepted: April 21, 2022. Date of CrossCheck: April 21, 2022. Date of online publication: June 8, 2022.

This work was supported by the National Natural Science Foundation of China (No. U2066601).

J. Xu, S. Liao (corresponding author), B. Xie, D. Ke, Y. Sun, X. Li, and X. Peng are with the School of Electrical Engineering and Automation, Wuhan University, Wuhan 430072, China (e-mail: xujian@whu.edu.cn; liaosiyang@whu.edu.cn; kedeping@whu.edu.cn; yzsun@mail.tsinghua.edu.cn; lixiong@whu.edu.cn; JYang@whu.edu.cn; hustpxt@whu.edu.cn).

H. Fu is with the Power Dispatching and Control Center of State Grid Jibei Electric Power Company Limited, Beijing 100054, China (e-mail: 641391917@qq.com).

DOI: 10.35833/MPCE.2021.000621

Common voltage regulating equipment includes power capacitors, on-load tap changers (OLTCs), and static synchronous compensators [13], [14]. However, the aforementioned voltage-regulating equipment discretely controls voltage, thus the load cannot be continuously regulated. A dynamic voltage restorer (DVR) is a device that is used to control the voltage in real time by changing the trigger angle of the inverter. Owing to its rapid and continuous voltage regulation characteristics, it is often used to solve voltage quality problems such as voltage flickers, fluctuations, and harmonic waves [15], [16]. Therefore, the DVR is used to regulate the voltage in real time to achieve load control in this study.

It is critical for scholars to determine a control method or strategy that achieves a rapid control of the load. Most existing studies use a single time-section control algorithm such as proportion-integration-differentiation (PID) algorithm [17], [18] without considering the coordination of multiple time sections to maximize the stabilization of PV power fluctuations. The model predictive control (MPC) algorithm [19], [20] is a process control algorithm, and its rolling optimization can fully consider the coordination of multiple time sections, thus having a certain prejudgment. The existing literature primarily uses MPC to control the voltage [21] and frequency [22] of the power grid. Since the voltage and frequency tend to be stable or only have a small fluctuation over time, the requirement for the accuracy of the prediction model is not high. However, when the control target such as active power is an indicator that does not tend to be stable, it is necessary to further improve the robustness of the prediction model or to add a feedback correction after the control, thereby ensuring control accuracy. A reasonable reference value of MPC can stabilize the PCC power fluctuation while ensuring that the voltage regulation has the least impact on the grid and user sides; therefore, the reference value needs to be optimized before control.

In summary, for smoothing the PV power fluctuations in the DN, this study presents a demand-side management strategy based on the MPC to continuously control the power of the feeder-level load through voltage regulation. Specifically, the voltage as the regulating resource is limited by the voltage qualification rate, and the voltage is reversly regulated ahead of the power fluctuations through the rolling optimization of MPC, thus the regulation capacity of the feeder-level load significantly increases during the occurrence of severe power fluctuations. The main contributions of this study are as follows.

1) A multi-time scale demand-side management strategy including pre-scheduling and real-time control for the suppression of PV power fluctuation is proposed. In the pre-scheduling, a multi-objective intraday optimization model is established to solve the reference power of the PCC. In the real-time control, the load power responds to the PV output through a feeder-level load control.

2) A rolling optimization method based on the MPC algorithm for voltage regulation is proposed. The controlled autoregressive integral moving average (CARIMA) based time series model is used to predict the power of the PCC in the short term. The parameters of the power prediction model are updated in real time to avoid the influence of PV or load randomness. With the prediction function of rolling optimization, the DVR will pre-regulate the voltage in advance when the power of the PCC is predicted to change abruptly to obtain a greater load regulation space when power fluctuation occurs.

The rest of the paper is organized as follows. The multi-time-scale demand-side management strategy for the suppression of PV power fluctuation is proposed in Section II. A case study of an industrial park in Guangzhou, China is used to verify the effectiveness of the strategy in Section III. Finally, the conclusions are drawn in Section IV.

II. Multi-time-scale Demand-side Management Strategy

A feeder-level load control method is first proposed in this section. The feeder voltage is continuously regulated by the DVR, which provides a control method for demand-side management. Second, a demand-side management strategy based on pre-dispatching and real-time control is established, which considers the smoothing of PCC power fluctuation as the ultimate goal for optimizing voltage regulation. Finally, the PCC power fluctuations caused by the PV system can be smoothed by a load control.

A. Feeder-level Control Method

1) Feeder-level Load Controllability Study

The static load model is currently often used to characterize the coupling relationship between the load power and voltage [9]. The static load model of the feeder in the DN can be expressed as:

$$P_f = P_{fN}\left[A_f\left(\frac{U_f}{U_{fN}}\right)^2 + B_f\frac{U_f}{U_{fN}} + C_f\right] \tag{1}$$

where A_f, B_f, and C_f are the proportions of the constant impedance load, constant current load, and constant power load in feeder f, respectively; U_f and U_{fN} are the real-time voltage and rated voltage of the feeder, respectively; and P_f and P_{fN} are the real-time active power and rated active power of the feeder, respectively. The coupling relationship between P_f and U_f is directly related to the proportion of the various loads at the feeder level.

To facilitate the description of the effect of voltage on the active power, the coupling coefficient between the voltage and active power of the feeder-level load (n_p^{FE}) is defined as:

$$n_p^{FE} = [(P_f - P_{f0})/P_{f0}]/[(U_f - U_{f0})/U_{f0}] \tag{2}$$

where P_{f0} and U_{f0} are the initial or reference values of the active power and voltage for each feeder, respectively.

The 10 kV feeder of the DN consists of multiple 380 V/220 V transformer districts, and the load type in each transformer district is generally the same. As shown in (1), the same load type has the same coupling coefficient; therefore, the coupling coefficient of the feeder-level load can be calculated by the coefficient of the load in each transformer district as follows:

$$n_p^{FE} = \sum_{c=1}^{D} n_{p,c}^{LD} \frac{P_c}{P_{total}} \tag{3}$$

where D is the total number of transformer districts in the feeder; $n_{p,c}^{LD}$ is the coupling coefficient between the load voltage and active power of transformer district c; P_c is the active power in district c; and P_{total} is the active power of the feeder.

Since the control cycle is short, the fluctuation of $n_{p,c}^{LD}$ is only affected by the season and law of production and life. The $n_{p,c}^{LD}$ of different load types in each season are summarized in [8] and [9]; for example, the $n_{p,c}^{LD}$ of the residential load in summer is 1.6, and the $n_{p,c}^{LD}$ of the commercial load in winter is 0.8. To verify the ability of the active power to vary with the voltage and measure the n_p^{FE} of the controlled feeder-level load, the DVR installed on site is used to regulate the voltage of the load, while the power of the feeder-level load is recorded. The n_p^{FE} value is calculated according to the field data and (2). The calculation results are presented in Table I, where ΔU is the change rate of feeder voltage after DVR regulation; and ΔP is the change rate of feeder active power after DVR regulation.

TABLE I
CALCULATION RESULTS OF COUPLING COEFFICIENT OF CONTROLLED FEEDER-LEVEL LOADS

ΔU (%)	ΔP (%)	n_p^{FE}
1.24	1.92	1.5484
1.22	2.00	1.6803
–1.25	–2.01	1.6080
–1.28	–1.99	1.5547
–1.27	–2.08	1.6378
–1.12	–1.69	1.5115

2) Modelling of DVR

The DVR is a voltage regulating device based on power electronic components and regulates the output voltage of the series transformer by changing the trigger angle of the inverter unit. Since the inverter angle can be continuously changed stepwise, the DVR can adjust the voltage quickly and continuously [23]. A DVR is composed of several power electronic devices, which cannot be considered in the original Jacobian matrix; therefore, it is necessary to establish an equivalent model according to the DVR function.

The circuit structure of the equivalent feeder with the DVR is shown in Fig. 1. The DVR is connected in series between nodes m and n in the original network. U_{se} and θ_{se} are the equivalent voltage and the voltage phase angle of the series transformer, respectively; U_h and θ_h are the equivalent voltage and the voltage phase angle of the parallel transformer of the DVR, respectively; X_s and X_h are the equivalent reactances of the DVR; G_{mn} and B_{mn} are the conductance and susceptance of the line, respectively; and b_c is the susceptance to the ground. The internal resistance of the transformer is ignored.

The DVR is a passive device, and the sum of the active power of the parallel and series branches is zero. To avoid the involvement of a voltage source and improve the speed of intraday optimization, the internal circuit model of the DVR can be simplified according to passive characteristics. The effect of DVR on the DN is manifested by the power injection at both ends of the original line nodes m and n [24]. The dual node power injection model of DVR is presented in Fig. 2.

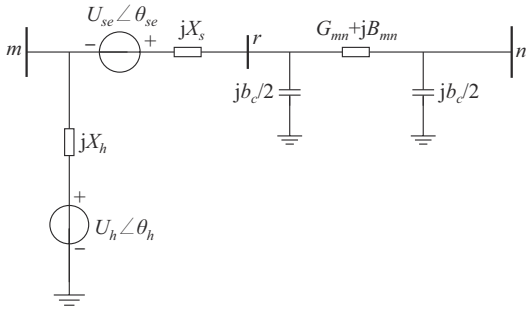

Fig. 1. Circuit structure of equivalent feeder with DVR.

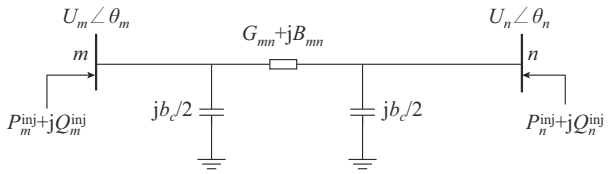

Fig. 2. Dual node power injection model of DVR.

The power injection of nodes m and n can be expressed as:

$$\begin{cases} P_m^{\text{inj}} = -\left(U_{se}^2 G_{mn} + 2U_m U_{se} G_{mn}\cos\theta_{mse}\right) + \\ \qquad U_{se}U_n\left(G_{mn}\cos\theta_{sen} + B_{mn}\sin\theta_{sen}\right) \\ Q_m^{\text{inj}} = -U_m U_{se}\left[G_{mn}\sin\theta_{mse} - \left(B_{mn} + \dfrac{b_c}{2}\right)\cos\theta_{mse}\right] \\ P_n^{\text{inj}} = U_n U_{se}\left(G_{mn}\cos\theta_{nse} + B_{mn}\sin\theta_{nse}\right) \\ Q_n^{\text{inj}} = U_n U_{se}\left(G_{mn}\sin\theta_{nse} - B_{mn}\cos\theta_{nse}\right) \end{cases} \tag{4}$$

where U_m and U_n are the voltage amplitudes on the input side and output side of the DVR access point, respectively; θ_{mse} and θ_{nse} are the differences between the voltage phase angles of nodes m and n and the voltage phase angle of equivalent series transformer in DVR, respectively; θ_{sen} is the difference between the voltage phase angle of equivalent series transformer and the voltage phase angle of node n; P_m^{inj} and Q_m^{inj} are the active power and reactive power injected by the DVR sending node, respectively; and P_n^{inj} and Q_n^{inj} are the active power and reactive power injected by the DVR receiving node, respectively.

Through the above modeling of the DVR, U_{se} and θ_{se} can be added to the power flow model in the pre-scheduling to express the influence of DVR on the feeder voltage. Since most of the wiring forms of the DN are radial, the DVR can be installed in the switch station at the sending end of the feeder to achieve the load control of the entire feeder.

B. Modelling of Pre-scheduling

The reference value of PCC power is an important input

of the MPC. Frequent voltage regulation significantly increases the network loss and affects the demand-side power. Therefore, a multi-objective intraday optimization model is established to solve the optimal power of the PCC. In the MPC, the optimal power is proportionally combined with the measured power to form the final reference value. A reasonable reference value can be used in the MPC to stabilize the fluctuations and minimize their impact on the DN. In this study, the process of calculating the optimal power of the PCC is called "pre-scheduling".

The PV output is significantly random, and the intraday prediction of a short-time scale has certain deviations. To reduce the influence of prediction deviation on optimization, the method proposed in [25] is used to cope with the stochasticity of the PV output, and the objective function with randomness is converted into the desired form.

An intraday optimization model is established to solve the reference power of the PCC in each pre-scheduling cycle. The objective function is divided into three parts. To smooth the PCC power fluctuation, the first part of the objective function minimizes the difference between the PCC power in each adjacent prescheduling cycle. The power regulation of the load is considered as the second part to improve the power supply quality and avoid the large-scale voltage regulation of the DVR. The transmission loss is considered as the third part of the objective function to minimize the power loss in the control. To conveniently describe the characteristics of the feeder-level load voltage control, this study neglects the electrical distance between the loads in each feeder and concentrates the loads on one node. The objective function is as follows.

$$\min E(f) = \sum_{s\in S}\pi_s\Bigg[\alpha\left(P^{\text{grid}}_{s,k}-P^{\text{grid}}_{s,k-1}\right)^2+\beta\sum_{f=1}^{N_F}\left(\Delta P^{\text{load}}_{s,f,k}\right)^2+\gamma P^{\text{loss}}_{s,k}\Bigg]\quad k=1,2,\ldots,N_D \tag{5}$$

where S is the total number of generated scenarios; π_s is the probability of scenario s; α, β, and γ are the weight coefficients of the power fluctuation, load power regulation, and transmission loss value in the objective function, respectively; $P^{\text{grid}}_{s,k}$ is the PCC active power in the pre-scheduling cycle k of scenario s; $\Delta P^{\text{load}}_{s,f,k}$ is the regulation value of the load active power of feeder f in the pre-scheduling cycle k of scenario s; N_F is the total number of feeder lines in the DN; $P^{\text{loss}}_{s,k}$ is the transmission loss in the pre-scheduling cycle k of scenario s; and N_D is the total number of pre-scheduling cycles.

The constraints for the objective function are as follows.

1) Balance constraint of active power

The injected power of nodes integrated into the DVR must be reflected in the equality constraint. The PCC power constraint is as follows:

$$\sum_{f=1}^{N_F}\left(P^{\text{load}}_{s,f,k}+\Delta P^{\text{load}}_{s,f,k}\right)-\sum_{m=1}^{N_B}\left(P^{\text{pv}}_{s,m,k}+P^{\text{inj}}_{s,m,k}\right)+P^{\text{loss}}_{s,k}=P^{\text{grid}}_{s,k} \tag{6}$$

where $P^{\text{load}}_{s,f,k}$ is the load active power of feeder f in the pre-scheduling cycle k of scenario s; $P^{\text{pv}}_{s,m,k}$ is the PV power of node m in the pre-scheduling cycle k of scenario s; $P^{\text{inj}}_{s,m,k}$ is the active power injected by the DVR sending node in the pre-scheduling cycle k of scenario s; and N_B is the number of system nodes.

2) Active power of feeder-level load

The relationship between the load power regulation and voltage regulation can be expressed as:

$$\Delta P^{\text{load}}_{s,f,k}=n^{FE}_{p,f}\Delta U_{s,f,k}\quad \forall f\in N_F \tag{7}$$

where $n^{FE}_{p,f}$ is the coupling coefficient between the voltage and active power of the load of feeder f; $\Delta U_{s,f,k}$ is the theoretical voltage regulation value of the DVR in the pre-scheduling cycle k of scenario s.

3) Power flow constraints

The DVR model is considered in the optimization model with the method indicated in Section II-C; therefore, the power flow constraints of the optimization model can be written as:

$$\begin{cases}P^{\text{pv}}_{s,m,k}+P^{\text{inj}}_{s,m,k}-P^{\text{load}}_{s,m,k}=\\ \qquad U_{s,m,k}\sum_{n=1}^{N_B}U_{s,n,k}\left(G_{mn}\cos\theta_{mn,k}+B_{mn}\sin\theta_{mn,k}\right)\\ Q^{\text{pv}}_{s,m,k}+Q^{\text{inj}}_{s,m,k}-Q^{\text{load}}_{s,m,k}=\\ \qquad U_{s,m,k}\sum_{n=1}^{N_B}U_{s,n,k}\left(G_{mn}\sin\theta_{mn,k}-B_{mn}\cos\theta_{mn,k}\right)\end{cases} \tag{8}$$

where $P^{\text{load}}_{s,m,k}$ is the load active power of node m in the pre-scheduling cycle k of scenario s; $Q^{\text{inj}}_{s,m,k}$ is the reactive power injected by the DVR sending node in the pre-scheduling cycle k of scenario s; $U_{s,m,k}$ and $U_{s,n,k}$ are the voltage amplitudes of nodes m and n in the pre-scheduling cycle k of scenario s, respectively; and $\theta_{mn,k}$ is the phase angle difference.

The power flow constraints include nonlinear models such as trigonometric functions. Therefore, the pre-scheduling model established in this paper is a nonlinear optimization one that can be solved using the TOMLAB toolbox in MATLAB. The $P^{\text{grid}}_{s,k}$ in each scenario s can be solved through the pre-scheduling model, and the mathematical expectation of $P^{\text{grid}}_{s,k}$ is $P^{\text{grid}}_{k,\text{opt}}$ which can be obtained from the probability of each scenario s and its corresponding $P^{\text{grid}}_{s,k}$. Finally, $P^{\text{grid}}_{k,\text{opt}}$ is the optimization result of the PCC. The $P^{\text{grid}}_{k,\text{opt}}$ and the measured PCC power are combined proportionally to form the reference value in the real-time control based on MPC.

C. Modelling of Real-time Control

In the real-time control, the voltage regulation of the DVR is solved using the MPC algorithm combined with pre-scheduling results, which can be suppressed through continuous load control.

1) Prediction Model

The advantage of the MPC over the traditional single-time scale control is that it uses the prediction value to perform rolling optimization for the control variable, thus the control has certain predictability. Therefore, the prediction of PCC power is an important part of the MPC. The PV output is closely related to the change in clouds at the previous moment, and the load power is also related to the previous moment. This study uses the CARIMA model with a static er-

ror elimination function to predict the PCC power in the ultra-short term [26] as follows:

$$\boldsymbol{A}\left(z^{-1}\right)\boldsymbol{P}_t^{\text{grid}}=\boldsymbol{B}\left(z^{-1}\right)\boldsymbol{U}_{t-1}+\frac{\boldsymbol{E}_t}{1-z^{-1}} \tag{9}$$

where $\boldsymbol{A}$ and $\boldsymbol{B}$ are the parameter matrices of the output and input, respectively, the dimension of $\boldsymbol{A}$ is $h\times h$, the dimension of $\boldsymbol{B}$ is $h\times N_F$, and h is the number of model input variables; the dimension of $\boldsymbol{P}_t^{\text{grid}}$ is $h\times 1$, $\boldsymbol{P}_t^{\text{grid}}=[P_{1,t}^{\text{grid}},P_{2,t}^{\text{grid}},\ldots,P_{h,t}^{\text{grid}}]^{\text{T}}$, and $P_{i,t}^{\text{grid}}$ is the active power of the i^{th} PCC; the dimension of $\boldsymbol{U}_{t-1}$ is $N_F\times 1$, $\boldsymbol{U}_{t-1}=[U_{1,t-1},U_{2,t-1},\ldots,U_{N_F,t-1}]^{\text{T}}$, and $U_{i,t-1}$ is the voltage amplitude of the i^{th} feeder; the dimension of disturbance variable $\boldsymbol{E}_t$ is $h\times 1$; and z^{-1} is the backward shift operator. In this paper, the PCC power is the unique input variable, thus h is 1. N_F is the number of feeders, which can be adjusted according to the case. The formulas after considering the backward shift operator are as follows.

$$\boldsymbol{A}\left(z^{-1}\right)=1+\boldsymbol{A}_1z^{-1}+\ldots+\boldsymbol{A}_{n_a}z^{-n_a} \tag{10}$$

$$\boldsymbol{B}\left(z^{-1}\right)=\boldsymbol{B}_0+\boldsymbol{B}_1z^{-1}+\ldots+\boldsymbol{B}_{n_b}z^{-n_b} \tag{11}$$

where $\boldsymbol{A}_i$ is the input matrix from time t to $t-n_a$, and its dimension is the same as $\boldsymbol{A}$; and $\boldsymbol{B}_i$ is the input matrix from time t to $t–n_b$, and its dimension is the same as $\boldsymbol{B}$. The n_a and n_b need to be set in advance according to the characteristics of the controlled system.

As shown in (9), the input and output values of each moment are coupled, and the PCC power cannot be directly predicted according to the feedback. Therefore, the Diophantine equation is further used to decouple the CARIMA model [27], so that the output can be predicted by using the input and output values at the current moment and the future ones can be forecasted. Ignoring the disturbance variable, the transformed optimal prediction model can be written as:

$$\boldsymbol{P}_{\text{grid}}=\sum_{f=1}^{N_F}\boldsymbol{G}_f\Delta\boldsymbol{U}_f+\boldsymbol{F}\boldsymbol{P}_{\text{grid}}^{his}+\sum_{f=1}^{N_F}\boldsymbol{H}_f\Delta\boldsymbol{U}_f^{his} \tag{12}$$

where $\boldsymbol{P}_{\text{grid}}=[P_{t+1}^{\text{grid}},P_{t+2}^{\text{grid}},\ldots,P_{t+N_1}^{\text{grid}}]^{\text{T}}$, N_1 is the prediction horizon length, and $P_{t+N_1}^{\text{grid}}$ is the predicted value of the PCC power at time $t+N_1$; $\Delta\boldsymbol{U}_f=[\Delta U_{f,t},\Delta U_{f,t+1},\ldots,\Delta U_{f,t+N_u-1}]^{\text{T}}$, N_u is the control horizon length, and $\Delta U_{f,t+N_u-1}$ is the predicted value of feeder voltage amplitude regualtion of feeder f at time $t+N_u-1$; $\Delta\boldsymbol{U}_f^{his}=[\Delta U_{f,t-1},\Delta U_{f,t-2},\ldots,\Delta U_{f,t-n_b}]^{\text{T}}$, and $\Delta U_{f,t-n_b}$ is the historical value of the feeder voltage amplitude regualtion of feeder f at time $t-n_b$; $\boldsymbol{P}_{\text{grid}}^{his}=[P_t^{\text{grid}},P_{t-1}^{\text{grid}},\ldots,P_{t-n_a+1}^{\text{grid}}]^{\text{T}}$, and $P_{t-n_a+1}^{\text{grid}}$ is the historical value of the PCC power at time $t-n_a+1$; and $\boldsymbol{G}_f$, $\boldsymbol{F}$, and $\boldsymbol{H}_f$ are the matrices introduced in the Diophantine equation, which can be deduced by matrices $\boldsymbol{A}$ and $\boldsymbol{B}$. The dimension of $\boldsymbol{G}_f$ is $N_1\times N_u$, the dimension of $\boldsymbol{F}$ is $N_1\times n_a$, and that of $\boldsymbol{H}_f$ is $N_1\times n_b$. The first term on the right side of (12) indicates the control excitation, and the latter two terms are the known initial conditions.

2) Rolling Optimization

For a highly random system, the system power significantly changes within 15 min. If the optimal power in the pre-scheduling is considered as the reference value of the MPC, it may lead to excessive load regulation. Therefore, to fully consider the current state of the system, the optimal power and measured power are proportionally combined to form the reference value of the MPC as follows.

$$\begin{cases}P_t^{\text{grid,ref}}=P_t^{\text{grid}}\\ P_{t+j}^{\text{grid,ref}}=\mu P_{k,\text{opt}}^{\text{grid}}+\left(1-\mu\right)P_{t+j-1}^{\text{grid,ref}}\quad j=1,2,\ldots,N_1\\ \mu=\dfrac{\tau}{\tau+T_c}\end{cases} \tag{13}$$

where τ is the filter time constant; T_c is the control period; j is the prediction time; $P_t^{\text{grid,ref}}$ is the reference value of the PCC active power; and $\mu\in[0,1]$ is the output softening coefficient. τ is proportional to μ; when τ increases, it indicates that the proportion of $P_{k,\text{opt}}^{\text{grid}}$ in $P_{t+j}^{\text{grid,ref}}$ increases, and the filtering effect on the PCC power fluctuations in the control is improved.

In the rolling optimization model of the MPC, the difference between the prediction power of the PCC and the reference value is considered as the first part of the objective function. To minimize the regulation of the demand-side power, the voltage regulation is considered as the second part of the objective function. The weight coefficient matrix in the objective function can reasonably distribute the weights of the power deviation and the control variables. The objective function and constraints are expressed as:

$$\begin{cases}\min\ J=\displaystyle\sum_{j=1}^{N_1}\lambda_j\left(P_{t+j}^{\text{grid}}-P_{t+j}^{\text{grid,ref}}\right)^2+\sum_{f=1}^{N_F}\sum_{j=1}^{N_u}\xi_{m,j}\Delta U_{f,t+j-1}^2\\ \text{s.t. }P_{t+j}^{\text{grid}}=\displaystyle\sum_{f=1}^{N_F}G_{f,j}\Delta U_{f,t+j-1}+F_jP_t^{\text{grid}}+\sum_{f=1}^{N_F}H_{f,j}\Delta U_{f,t-1}\\ U_{f,t+1}=U_{f,t}+\Delta U_{f,t}\\ U_{\min}\le U_{f,t}\le U_{\max}\\ R_t=\left(P_t^{\text{grid}}-P_{t-1}^{\text{grid}}\right)\big/P_{t-1}^{\text{grid}}\\ \left(1-R_{\max}\right)P_{t+j-1}^{\text{grid}}\le P_{t+j}^{\text{grid}}\le\left(1+R_{\max}\right)P_{t+j-1}^{\text{grid}}\end{cases} \tag{14}$$

where λ_j and $\xi_{m,j}$ are the weight coefficients of the PCC power deviation and the voltage regulation, respectively; $G_{f,j}$, F_j, and $H_{f,j}$ are the elements of $\boldsymbol{G}_f$, $\boldsymbol{F}$, and $\boldsymbol{H}_f$, respectively; $U_{f,t}$ is the voltage amplitude of the f^{th} feeder at time t; $U_{\max}$ and $U_{\min}$ are the maximum and minimum voltage amplitudes allowed by the current DN, respectively; R_t is the active power fluctuation rate of PCC at time t; and $R_{\max}$ is the allowable maximum value of the active power fluctuation rate of PCC, which is considered as 10% per min in this study. Formula (14) is a quadratic programming problem, which can be solved by toolboxes such as CPLEX in MATLAB.

Online rolling optimization is the core of demand-side management strategy. The $\Delta U_{f,t+j-1}$ of the objective function from a current state to the control horizon N_u is solved by (14), and then $\Delta U_{f,t}$ is taken as the DVR voltage regulation value of the f^{th} feeder at time t. According to $\Delta U_{f,t}$ and $U_{f,t}$ at time t, the feeder voltage $U_{f,t+1}$ at time $t+1$ can be obtained by summing them.

The rolling optimization of the MPC can achieve the effect of pre-regulation. When the PCC power is predicted to decrease at time t, i.e., the PV output increases sharply at time t, the DVR reduces the voltage from $t-N_u$ to $t-N_u+1$

in advance without exceeding the original power volatility limit. Thus, a larger voltage rising space and greater regulation power of the load based on the voltage qualification rate at time t can be obtained. Similarly, when the PCC power is predicted to rise sharply at time t, the DVR raises the voltage from $t-N_u$ to $t-N_u+1$ in advance. Thus, a larger voltage dropping space at time t can be obtained. Therefore, the predictive function of the MPC can make better use of the regulable demand-side capacity compared with the single-timescale control, thereby achieving a wider range of power suppression.

3) Feedback Correction

The stochasticity of the PV and load causes the CARIMA model to inaccurately predict the PCC power. To improve the self-adaptability of the prediction model, the parameters of the CARIMA model are identified online by substituting the calculated control variables and real-time feedback PCC power into the recursive least squares (RLS) model. Therefore, the prediction model updates the parameters according to the system state at the previous moment in each control cycle, avoiding the influence of external random variables on the control algorithm and further improving the control accuracy.

Based on the aforementioned analysis, the overall real-time control is as follows: ① the difference between P_{t+j}^{grid} and $P_{t+j}^{\text{grid,ref}}$ is considered as the input; ② the voltage regulation of each feeder $\Delta U_{f,t}$ is used as the control variable; ③ the PCC power after the control is obtained by adding the regulation value of each feeder-level load $\Delta P_{f,t}^{\text{load}}$, the PV power P_{PV}, and the basic power $P_{\text{basic}}^{\text{load}}$, which has no regulation ability. Before the start of each control cycle, the RLS method is used based on P_t^{grid} and $\boldsymbol{U}_t=[U_{1,t}, U_{2,t}, \ldots, U_{f,t}]^{\text{T}}$ to identify the parameters of the CARIMA model online and further predict the PCC power. The control block diagram based on the MPC is shown in Fig. 3.

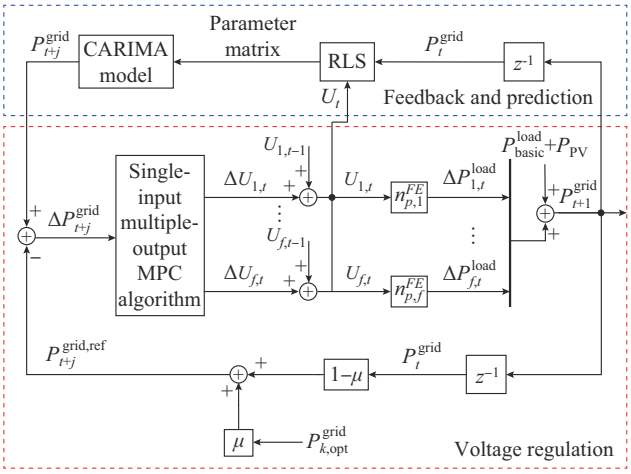

Fig. 3. Control block diagram based on MPC.

III. Case Study

A. Basic Data

The studied DN model is an actual power system in Guangzhou, China, as shown in Fig. 4. The distributed PV is integrated into F3 and F4 feeders, and DVRs are installed at the sending end of the F2 and F5 feeders, respectively. The rated load of each feeder is as follows: 4.6 MW for F1, 7.25 MW for F2, 2.38 MW for F3, 3.45 MW for F4, 1.52 MW for F5, and 3.68 MW for F6. The installed capacity of the PV in F3 and F4 is 4 MW, and the PV penetration of the DN model is 35%.

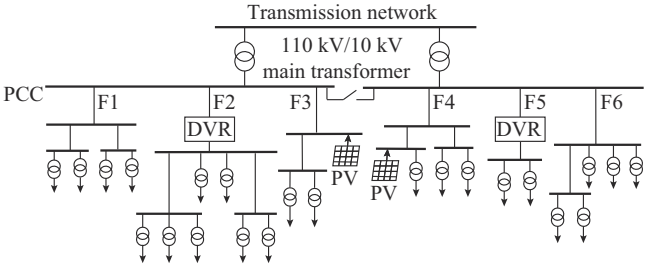

Fig. 4. DN model of an actual power system in Guangzhou, China.

Based on the method for calculating the coupling coefficient of the feeder, the n_p^{FE} is solved using (3). The load types and coupling coefficients of the feeders are listed in Table II.

TABLE II
Load Types and Coupling Coefficients of Feeders

Feeder	Main load type	Capacity (MW)	$n_{p,c}^{LD}$	n_p^{FE}
F2	Asynchronous motor	2.20	1.5	1.59
	Residential	2.25	1.6	
	Shopping mall	2.80	0.8	
F5	Agricultural	0.80	0.6	1.07
	Residential	0.72	1.6	

B. Model Solving

The high stochasticity of the PV power in the DN model is the main factor affecting the PCC power fluctuations. The PV power data in a winter day in Guangzhou, China are selected as the data of PV active power in the real-time control model, as shown in Fig. 5.

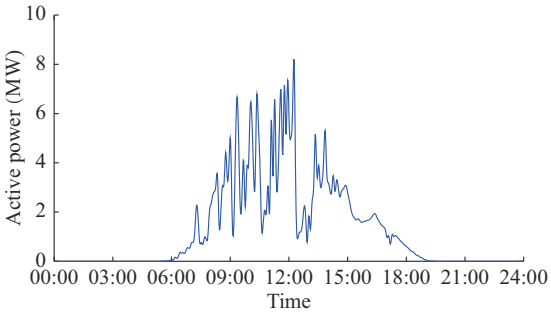

Fig. 5. PV power data in a winter day in Guangzhou, China.

As shown in Fig. 5, the PV power fluctuates sharply during 08:30 to 16:30. To highlight the effect of suppressing power fluctuations, the demand-side management strategy is implemented in these eight hours. First, $P_{k,\text{opt}}^{\text{grid}}$ is solved by pre-scheduling, and the weight coefficients of the objective function in pre-scheduling are set as $\alpha=2$, $\beta=5$, and $\gamma=3$.

The resolution time of the existing ultra-short-term load

prediction data is 15 min, and according to the maximum resolution time of the power prediction data, the pre-scheduling period is set to be 15 min. As shown in Fig. 6, when the PCC power volatility is predicted to be less than 10% per min, the DVR does not participate in the voltage regulation; thus, the PCC active power is the same before and after the optimization. The PCC active power is smoothed by the optimization when the PCC power volatility exceeds 10% per min.

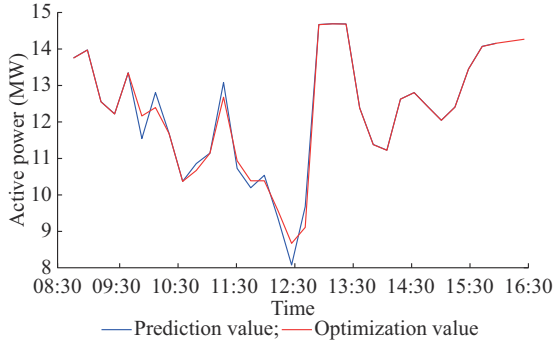

Fig. 6. Comparison of PCC active power.

To meet the requirements of the standard GB/T 19964-2012 and other provisions, the maximum value of the PCC power volatility is 10% per min. Therefore, the control period T_c is 1 min, which meets the provisions of relevant regulations. According to Fig. 6, h is set to be 1 and N_F is set to be 2. According to the complexity of the CARIMA model, n_a is set to be 11 and n_b is set to be 5. In the parameter setting of the MPC, the prediction horizon N_1 is 5 min, the control horizon N_u is 3 min, and the filter time constant τ is 5 min. A comparison of the PCC active power before and after the control is shown in Fig. 7. A comparison of the PCC power volatility is shown in Fig. 8. The voltage at the sending end of F2 and F5 after the control is shown in Fig. 9. A comparison of the active power of F2 and F5 is shown in Fig. 10.

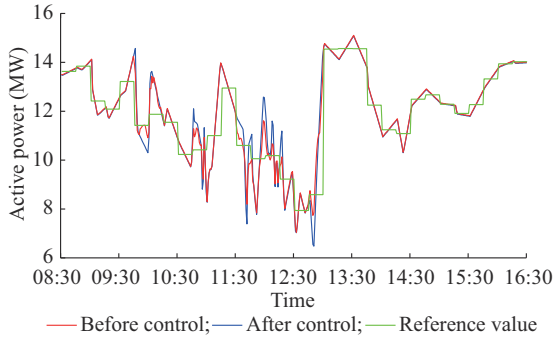

Fig. 7. Comparison of PCC active power before and after control.

The demand-side management can better suppress fluctuations of the PCC active power, as shown in Figs. 7 and 8. In addition, the DVR does not take part in the control when the power fluctuation is small, thereby ensuring a smoothing effect while significantly reducing the transmission loss caused by the DVR. The current measurement result of the PCC power is considered in the reference value of the MPC, such that the inherent fluctuation is restrained without additional power fluctuation. Prior to the control, there are 21 moments when the volatility exceeds 10% per min. After the control, the maximum volatility is reduced from 31% per min to 9.6% per min, which meets the requirement of the PCC power volatility not exceeding 10% per min.

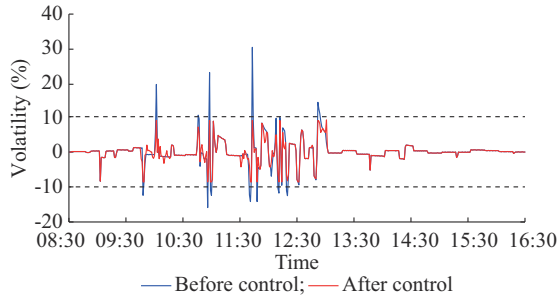

Fig. 8. Comparison of PCC power volatility.

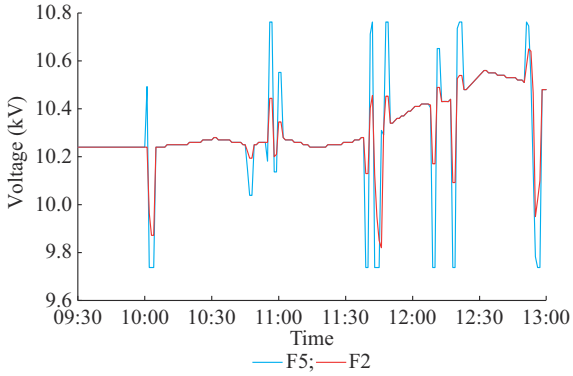

Fig. 9. Comparison of voltages at sending ends of of F2 and F5 after control.

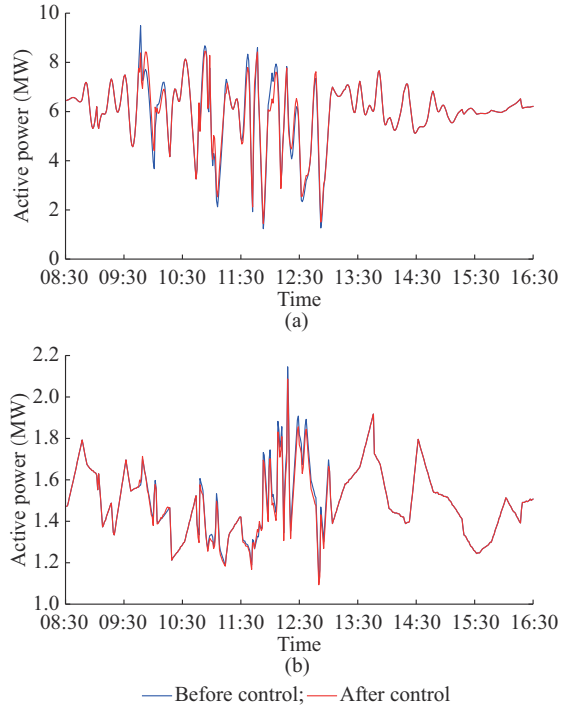

Fig. 10. Comparison of active power of F2 and F5. (a) Active power of F2. (b) Active power of F5.

To highlight the effect of voltage regulation during the violent power fluctuation, the voltage curve shown in Fig. 9 is selected for analysis. The n_P^{FE} of F2 is larger; therefore, its range of voltage regulation is significantly smaller than that of F5 in response to the same power fluctuation. F5 can only improve load regulation by increasing the range of the voltage regulation. When the power violently fluctuates, e.g., during 11:30 to 12:00, the feeder voltage is reversely regulated in advance before the power fluctuates to obtain a larger voltage regulation space during the power fluctuation. Similarly, because n_P^{FE} of F2 is larger than that of F5, F2 does not need to obtain a larger load regulation space through reverse regulation at certain time, thus the degree and times of the F5 reverse voltage regulation are larger than those of F2.

As shown in Fig. 10, the active power of the controlled feeder responds to the voltage of the DVR in real time, which is based on the voltage/power coupling characteristics. Through feeder-level load control, the PCC power fluctuation can be stabilized by each controlled feeder.

Based on the aforementioned results, the PCC power fluctuation can be significantly reduced by ensuring the voltage qualification rate through the demand-side management strategy. This strategy effectively avoids the PV curtailment caused by the PV power ramp by using the regulation potential of the load and improves the utilization rate of the PV.

The quadratic programming model established for real-time control consists of several practical solution tools. In this study, YALMIP and CPLEX toolboxes are used to solve this model. The model is solved in MATLAB R2016b through AMD Ryzen 5 4600H with a Radeon graphics 3.00 GHz processor and 16 GB RAM memory. The calculation time used in the real-time control is recorded, and the frequency and cumulative percentage of the calculation time in each control period are counted. The statistical results are shown in Fig. 11, which demonstrate that the maximum calculation time does not exceed 0.9 s, and the average calculation time is 0.67 s.

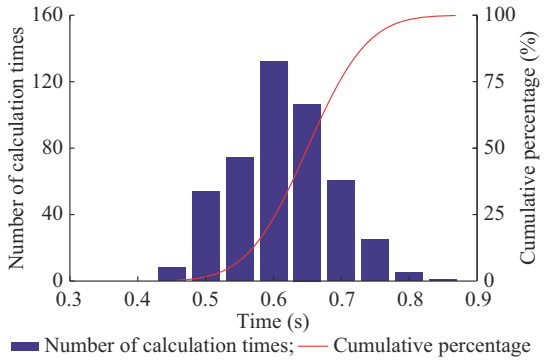

Fig. 11. Statistical results of time consumption of real-time control.

The constraints in the optimization model established by the pre-scheduling include nonlinear constraints such as power flow in the DN. In this study, YALMIP and TOMLAB toolboxes are used to solve the nonlinear programming problem, and the calculation is conducted by a computer and software with the same configuration as the real-time control. The average solution time of the pre-scheduling model is 32 s, much less than 15 min, which can also meet the time requirements of subsequent real-time control.

C. Comparison of Control Effect Between MPC Algorithm and PID Control Algorithm

The MPC algorithm applied in this study is an iterative control algorithm that determines the future voltage control regulation in the control horizon according to the predicted power of the PCC in the prediction horizon, and the PID control algorithm is a non-iterative control algorithm that calculates the voltage regulation value according to the PCC power deviation at current moment. In this subsection, based on the fact that the pre-scheduling results are consistent, the control effects of MPC algorithm and PID control algorithm are compared in the scenario with the same PV penetration rate and the scenario with different PV penetration rates.

1) Scenario with the Same PV Penetration Rate

In this scenario, the MPC algorithm and PID control algorithm are used to calculate the voltage regulation values, and the time period with an apparent control effect is intercepted for display. The comparison results are presented in Figs. 12-14.

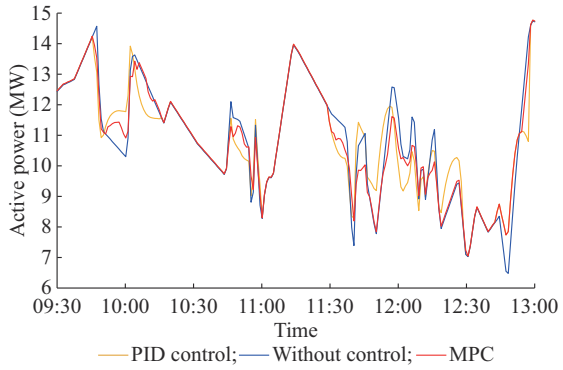

Fig. 12. Comparison of PCC active power with different control algorithms.

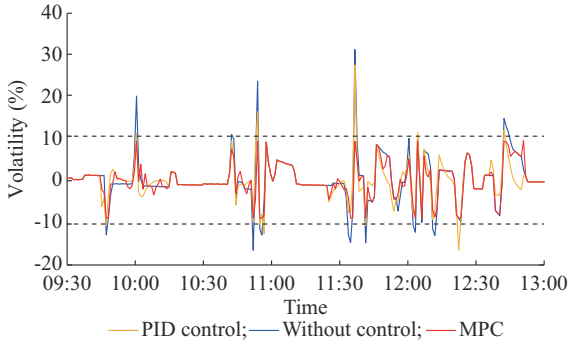

Fig. 13. Comparison of PCC power volatility with different control algorithms.

The MPC algorithm is superior to the PID control algorithm in smoothing fluctuations, as shown in Figs. 12 and 13. The PID control algorithm is a scale control algorithm that rapidly responds to the difference between the measurement power and the reference power of the PCC; however, it cannot sufficiently suppress the power fluctuation only by using the control at this time owing to the limitation of the voltage qualification rate when the power fluctuation is large.

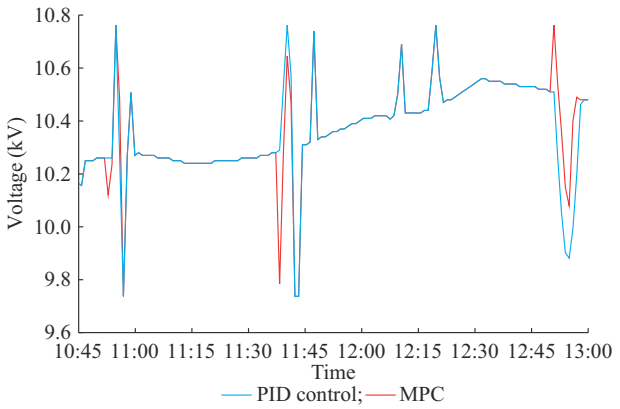

Fig. 14. Comparison of feeder F2 voltage amplitude with different control algorithms.

As shown in Figs. 12-14, the CARIMA model predicts that the PCC power is close to decreasing at approximately 11:40, and the MPC algorithm can obtain a larger voltage rising space when the PCC power decreases by reducing the voltage in advance without making the R_t at the current moment exceed the limitation, thereby achieving a larger range of power fluctuation stabilization. However, if the PID control algorithm raises the voltage to the upper limit when the PCC power rapidly decreases, the power fluctuation rate of the PCC cannot be controlled to be less than 10% per min. Similarly, at 12:55, the MPC algorithm increases the voltage in advance to obtain more space for voltage reduction when the PCC power increases.

Based on the aforementioned analysis indicating that non-iterative algorithms such as PID control algorithm only calculate the voltage regulation value of a single-time scale based on the current-moment output, the control effect of the traditional non-iterative algorithm is poor in a system with a large randomness. As shown in Fig. 13, although the PCC power fluctuation is reduced to a certain extent, the moments when the R_t is not controlled within 10% per min remain.

The advantage of the iterative algorithms such as MPC algorithm is that it can constantly modify its control quantity through the control effect. The MPC algorithm considers prediction data such as the PV power and load; therefore, the calculated control results have a certain predictability. The MPC algorithm reversely regulates the voltage before the PV power is predicted to fluctuate; thus, it has a larger voltage regulation space when the power violently fluctuates and achieves a larger range of power fluctuation suppression.

Considering the calculation time, the calculation model of the non-iteration algorithm is simple. Utilizing the computer and software with the same configurations indicated above, the average calculation time of the PID control algorithm is 0.23 s, which is less than that of the MPC algorithm. However, when suppressing minute-level power fluctuations, the calculation time of the MPC algorithm can also meet the requirements, and the MPC algorithm can provide a larger adjustable load power under the same constraints; therefore, the MPC algorithm has apparent advantages.

2) Scenario with Different PV Penetration Rates

The PV penetration rate directly affects the power fluctuation range of the PCC; therefore, it is selected as a single control variable. The MPC algorithm and PID control algorithm are used for the demand-side management, and the power fluctuation rate of the PCC is used as the evaluation index of the two control algorithms.

The PV penetration rate is the ratio of the installed PV capacity to the rated load capacity of the DN, and the PV penetration rate PV_{pe} is changed by adding the installed PV capacity. The PCC power fluctuations after the MPC and PID control are expressed using a probability density function (PDF). The PID and MPC algorithms are used to smooth the PCC power under the scenarios with PV penetration rates of 45%, 54%, and 68%, respectively. The PDF curve of R_t in each PV penetration rate scenario is shown in Fig. 15.

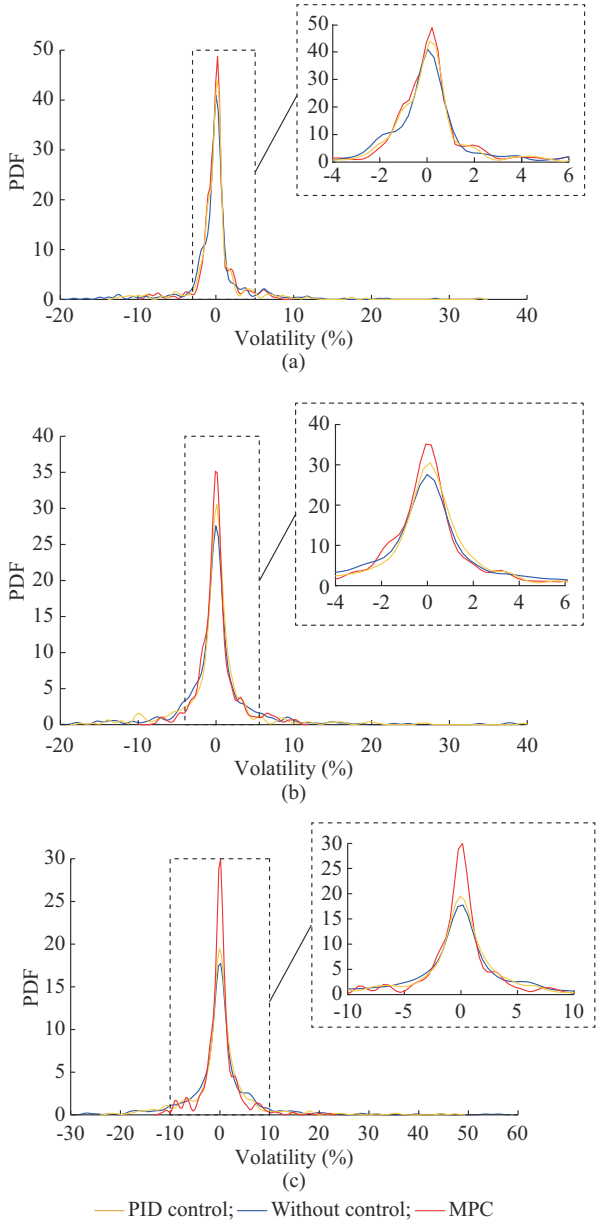

Fig. 15. PDFs of PCC power fluctuations for 45%, 54%, and 68% PV penetration rates. (a) 51% PV penetration rate. (b) 64% PV penetration rate. (c) 68% PV penetration rate.

When the system power flow meets the constraint, whether the maximum volatility exceeds 10% per min is the standard for determing whether the PV can be integrated into the DN under this capacity. The comparision of the effects after using different control algorithms is listed in Table III.

TABLE III
COMPARISON OF EFFECTS AFTER USING DIFFERENT CONTROL ALGORITHMS

PV capacity (MW)	PV_{pe} (%)	$R_{t,\max}$ after using MPC (%)		$R_{t,\max}$ after using PID (%)		Is it integrated into DN?
		Lower limit	Upper limit	Lower limit	Upper limit	
8	35	9.5	9.6	17	29	Yes
10	45	9.7	9.8	18	36	Yes
12	54	10.2	11.5	22	41	No
15	68	12.2	22.4	28	57	No

As shown in Fig. 15, when the penetration rate increases from 35% to 68%, the PCC power volatility increases from 31% per min to 58% per min without any control algorithm. The probability of the PCC power volatility distributed near 0 increases after using the control algorithms, indicating that the two algorithms have effectively stabilized the PCC power fluctuations to a certain extent. However, the number of volatilities distributed near 0 after using the MPC algorithm is larger than that of the PID control algorithm, and the volatility peak after using the MPC algorithm is also lower than that of the PID control algorithm. Therefore, the MPC algorithm has a better control effect than the PID control algorithm with different penetration rates.

The PID control algorithm is a single-time section control algorithm, which is limited by the voltage regulation range at the preceding time, and has a poor control effect during the time with the high power volatility. The MPC algorithm can pre-regulate the DVR voltage in advance according to the prediction power of the PCC; therefore, it has a larger load power regulation capacity than that of the PID control algorithm at the time with large power fluctuations. As shown in Fig. 15(b), when the installed PV capacity increases to 10 MW, the MPC algorithm can limit the PCC power volatility to 10% per min. However, when the installed PV capacity increases to 12 MW, the load power cannot fully smoothen the PV power fluctuation owing to the limitation of the voltage qualification rate, as shown in Fig. 15(c).

Based on the aforementioned results, the MPC algorithm uses the advantage of rolling optimization to make full use of the demand-side regulation ability, and its suppression effect with different PV penetration rates is better than that of the PID control algorithm. Therefore, the proposed strategy can smooth the PV power fluctuations in a wider range and further improve the PV utilization under the same regulation capacity.

IV. CONCLUSION

A multi-time-scale demand-side management strategy based on the MPC is proposed for the problem of PCC power fluctuations when there is a high penetration of distributed PV. The effectiveness of the proposed strategy in stabilizing the PCC power fluctuation is verified using an example. It also provides a solution to the problem that the DN cannot be connected to a distribution PV with larger capacity due to the power fluctuation rate of PCC exceeding the limit.

The following conclusions can be drawn from this study: ① the feeder voltage is regulated by the DVR to achieve the continuous regulation of the feeder-level load; ② in pre-scheduling, a multi-objective intraday optimization model is established to solve the reference value of the PCC; ③ based on the MPC, the voltage regulation is solved by the rolling optimization, and the DVR regulates the voltage prior to the PV ramp increasing based on the prediction, which enlarges the range of smoothing the PV power fluctuation; and ④ the MPC can smooth a wider range of power fluctuations than the PID control with a limited regulation capacity.

Finally, as advanced measurement devices are gradually integrated into the DN, the prediction and optimization model of MPC should be further improved in future studies to adapt to high-frequency control speeds.

REFERENCES

[1] J. Xu, B. Xie, S. Liao *et al*., "Load shedding and restoration for intentional island with renewable distributed generation," *Journal of Modern Power Systems and Clean Energy*, vol. 9, no. 3, pp. 612-624, May 2021.
[2] M. J. E. Alam, K. M. Muttaqi, and D. Sutanto, "A novel approach for ramp-rate control of solar PV using energy storage to mitigate output fluctuations caused by cloud passing," *IEEE Transactions on Energy Conversion*, vol. 29, no. 2, pp. 507-518, Mar. 2014.
[3] S. Shivashankar, S. Mekhilef, H. Mokhlis *et al*., "Mitigating methods of power fluctuation of photovoltaic (PV) sources – a review," *Renewable and Sustainable Energy Reviews*, vol. 59, pp. 1170-1184, Jun. 2016.
[4] N. Kakimoto, H. Satoh, S. Takayama *et al*., "Ramp-rate control of photovoltaic generator with electric double-layer capacitor," *IEEE Transactions on Energy Conversion*, vol. 24, no. 2, pp. 465-473, Sept. 2009.
[5] V. Gevorgian and S. Booth. (2013, Nov.). Review of PREPA technical requirements for interconnecting wind and solar generation. [Online]. Available: http://www.nrel.gov/publications
[6] D. Prudhviraj, P. B. S. Kiran, and N. M. Pindoriya, "Stochastic energy management of microgrid with nodal pricing," *Journal of Modern Power Systems and Clean Energy*, vol. 8, no. 1, pp. 102-110, Jan. 2020.
[7] T. V. Thang, A. Ahmed, C. Kim *et al*., "Flexible system architecture of stand-alone PV power generation with energy storage device," *IEEE Transactions on Energy Conversion*, vol. 30, no. 4, pp. 1386-1396, Dec. 2015.
[8] C. J. Lin, A. Y. T. Chen, C. Y. Chiou *et al.*, "Dynamic load models in power systems using the measurement approach," *IEEE Transactions on Power Systems*, vol. 8, no. 1, pp. 309-315, Feb. 1993.
[9] W. W. Price, H. D. Chiang, H. K. Clark *et al.*, "Load representation for dynamic performance analysis," *IEEE Transactions on Power Systems*, vol. 8, no. 2, pp. 472-482, May 1993.
[10] K. Mckenna and A. Keane, "Open and closed-loop residential load models for assessment of conservation voltage reduction," *IEEE Transactions on Power Systems*, vol. 32, no. 4, pp. 2995-3005, Oct. 2016.
[11] Z. Wang, B. Chen, J. Wang *et al.*, "Stochastic DG placement for conservation voltage reduction based on multiple replications procedure," *IEEE Transactions on Power Delivery*, vol. 30, no. 3, pp. 1039-1047, Jun. 2015.
[12] B. R. Scalley and D. G. Kasten, "The effects of distribution voltage reduction on power and energy consumption," *IEEE Transactions on Education*, vol. 24, no. 3, pp. 210-216, Aug. 1981.
[13] B. Singh, S. S. Murthy, and S. Gupta, "Analysis and design of STATCOM-based voltage regulator for self-excited induction generators," *IEEE Transactions on Energy Conversion*, vol. 19, no. 4, pp. 783-790, Dec. 2004.

[14] J. Ye and H. B. Gooi, "Phase angle control based three-phase DVR with power factor correction at point of common coupling," *Journal of Modern Power Systems and Clean Energy*, vol. 8, no. 1, pp. 179-186, Jan. 2020.
[15] R. Zhu, F. Deng, C. Zhe *et al*., "Enhanced control of DFIG wind turbine based on stator flux decay compensation," *IEEE Transactions on Energy Conversion*, vol. 31, no. 4, pp. 1366-1376, Dec. 2016.
[16] A. Ghosh and G. Ledwich, "Compensation of distribution system voltage using DVR," *IEEE Transactions on Power Delivery*, vol. 17, no. 4, pp. 1030-1036, Oct. 2002.
[17] S. Liao, X. Jian, Y. Sun *et al.*, "Load-damping characteristic control method in an isolated power system with industrial voltage-sensitive load," *IEEE Transactions on Power Systems*, vol. 31, no. 2, pp. 1-11, Mar. 2015.
[18] I. de la Parra, J. Marcos, M. Garcia *et al.*, "Control strategies to use the minimum energy storage requirement for PV power ramp-rate control," *Solar Energy*, vol. 111, pp. 332-343, Jan. 2015.
[19] X. Dou, J. Wang, Z. Wang *et al*., "A dispatching method for integrated energy system based on dynamic time-interval of model predictive control," *Journal of Modern Power Systems and Clean Energy*, vol. 8, no. 5, pp. 841-852, Sept. 2020.
[20] Y. Du, W. Pei, N. Chen *et al*., "Real-time microgrid economic dispatch based on model predictive control strategy," *Journal of Modern Power Systems and Clean Energy*, vol. 5, no. 5, pp. 787-796, Sept. 2017.
[21] T. John and S. P. Lam, "Voltage and frequency control during microgrid islanding in a multi-area multi-microgrid system," *IET Generation, Transmission & Distribution*, vol. 11, no. 6, pp. 1502-1512, Apr. 2017.
[22] H. Jiang, J. Lin, Y. Song *et al.*, "MPC-based frequency control with demand-side participation: a case study in an isolated wind-aluminum power system," *IEEE Transactions on Power Systems*, vol. 30, no. 6, pp. 3327-3337, Dec. 2015.
[23] C. Lam, M. Wong, and Y. Han, "Voltage swell and overvoltage compensation with unidirectional power flow controlled dynamic voltage restorer," *IEEE Transactions on Power Delivery*, vol. 23, no. 4, pp. 2513-2521, Oct. 2008.
[24] M. Noroozian, L. Angquist, M. Ghandhari *et al.*, "Use of UPFC for optimal power flow control," *IEEE Transactions on Power Delivery*, vol. 12, no. 4, pp. 1634, Oct. 1997.
[25] J. Dupacova, N. Growe-Kuska, and W. Romisch, "Scenario reduction in stochastic programming: an approach using probability metrics," *Mathematical Programming: Series B*, vol. 95, no. 3, pp. 493-511, Jan. 2003.
[26] B. W. Hogg and N. M. El-Rabaie, "Multivariable generalized predictive control of a boiler system," *IEEE Transactions on Energy Conversion*, vol. 6, no. 2, pp. 282-288, Jun. 1991.
[27] M. Clausen and F. Albrecht, "Efficient solution of linear diophantine equations," *Journal of Symbolic Computation*, vol. 8, no. 1-2, pp. 201-216, Jul. 1989.

Jian Xu received the B.S. and Ph.D. degrees in electrical engineering from Wuhan University, Wuhan, China, in 2002 and 2007, respectively. He is currently a Professor with the School of Electrical Engineering and Automation, Wuhan University. His research interests include power system operation, voltage stability, and wind power control and integration.

Haobo Fu received the B. S. and M. D. degrees in electrical engineering from Wuhan University, Wuhan, China, in 2017 and 2020, respectively. He is currently the Chief Dispatcher of the State Grid Jibei Electric Power Co., Ltd., Beijing, China. His research interests include power system operation, renewable energy, and load control.

Siyang Liao received the B. S. and Ph. D. degrees in electrical engineering from Wuhan University, Wuhan, China, in 2011 and 2016, respectively. He is currently an Associate Professor with the School of Electrical Engineering and Automation, Wuhan University. His research interests include wind power integration and power system simulation technology.

Boyu Xie received the B.S. degree in electrical engineering from Wuhan University, Wuhan, China, in 2017. He is currently working toward the Ph. D. degree in the School of Electrical Engineering and Automation, Wuhan University. His research interests include distribution system operation, renewable energy, and load control.

Deping Ke received the B. S. degree in electrical engineering from Huazhong University of Science and Technology, Wuhan, China, and the Ph. D. degree in electrical engineering from Hong Kong Polytechnic University, Hong Kong, China, in 2005 and 2012, respectively. He is currently an Associate Professor with the School of Electrical Engineering and Automation, Wuhan University, Wuhan, China. His research interests include power system dynamics and control and economical operation of power systems.

Yuanzhang Sun received the Ph.D. degree in electrical engineering from Tsinghua University, Beijing, China, in 1988. He is currently a Professor with the School of Electrical Engineering and Automation, Wuhan University, Wuhan, China, and a Chair Professor with the Department of Electrical Engineering and Vice Director of the State Key Laboratory of Power System Control and Simulation, Tsinghua University. His research interests include power system dynamics and control, voltage stability and control, and reliability.

Xiong Li received the Ph.D. degree from Tsinghua University, Beijing, China, in 1997. He is an Associate Professor with Wuhan University, Wuhan, China. His main research interests are in power system control based on wide area measurement system.

Xiaotao Peng received the B.S. degree in control engineering, and the M.S. and Ph. D. degrees in electrical engineering from the Huazhong University of Science and Technology, Wuhan, China, in 1993, 2002, and 2006, respectively. He is currently an Associate Professor with the School of Electrical Engineering and Automation, Wuhan University, Wuhan, China. His research interests include power system stability analysis and control, renewable energy, high-voltage direct current, and application of energy storage system.